JACS
JOURNAL OF THE AMERICAN CHEMICAL SOCIETY
Article
pubs.acs.org/JACS

Curved Polycyclic Aromatic Molecules That Are π-Isoelectronic to Hexabenzocoronene

Jiye Luo,[†] Xiaomin Xu,[†] Renxin Mao,[†] and Qian Miao*[,†,‡]

[†]Department of Chemistry, The Chinese University of Hong Kong, Shatin, New Territories, Hong Kong, China
[‡]Institute of Molecular Functional Materials (Areas of Excellence Scheme, University Grants Committee), Hong Kong, China

Supporting Information

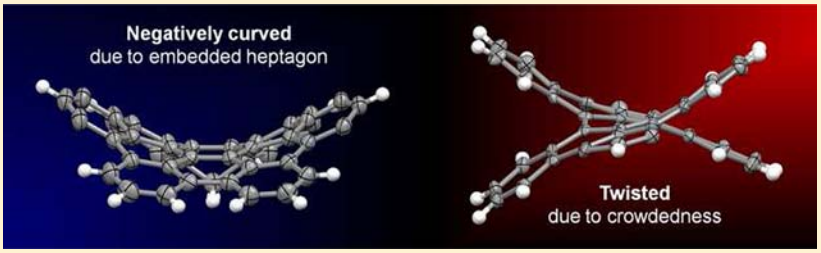

ABSTRACT: Reported here are two types of curved π-molecules that are π-isoelectronic to planar hexabenzocoronene (HBC) but are forced out of planarity either by an embedded seven-membered ring or by atom crowding at the fjord region. Embedding a heptagon in HBC leads to a novel saddle-shaped molecule **1**, whose π-backbone is slightly less curved than the previously reported [7]circulene in terms of the average Gauss curvature, but surprisingly much more rigid than [7]circulene. Overcrowded fjord regions in novel derivatives of hexabenzoperylene (HBP) **2a**,**b** lead to both chiral twisted and antifolded conformers. The successful synthesis of **1** and **2a**,**b** is related to introducing alkoxyl groups to unprecedented positions of hexaphenylbenzenes. It is found that the red twisted isomer of **2b** isomerizes at elevated temperature to the yellow *anti*-folded conformer. This finding along with the study on the thermodynamics and kinetics of the thermal isomerization has improved the early understandings on the conformation of HBP. In the crystals, **1** lacks π−π interactions between neighboring molecules, while twisted-**2a** exhibits both face-to-face and edge-to-face π−π interactions. Twisted-**2b** is found to function as a p-type semiconductor in thin film transistors, but the thin films of **1** appear insulating presumably due to lacking π−π interactions. By exploring three different types of curvatures in **1** and the two isomers of **2b**, this study has revealed that the curvature of π-face plays a role in determining the frontier molecular orbital energy levels and π−π interactions and thus needs to be considered when one designs new organic semiconductors.

INTRODUCTION

Polycyclic aromatic hydrocarbon (PAHs) molecules can be forced into nonplanar structures commonly either by embedded nonhexagonal rings[1] or by steric strain from atom crowding.[2] As shown in Figure 1a, reported here are curved large polycyclic aromatic compounds that are π-isoelectronic to the well-known planar hexa-*peri*-hexabenzocoronene (HBC)[3] but are forced out of planarity by the two strategies.

Embedding five-membered rings into an otherwise flat PAH molecule can lead to curved PAH molecules known as aromatic bowls,[4] (or buckybowls[6]), which not only serve as segments and model compounds for fullerene structure and reactivity[4−6] but also are used as synthetic precursors for synthesis of isomerically pure fullerenes[7] and carbon nanotubes.[8] In contrast to pentagon-embedded PAHs containing positive curvature, heptagon-embedded PAHs can give rise to negative curvature.[9,10] The interests on sp^2 carbon structures containing negative curvature can be traced back to theoretical[11] and experimental studies[12] on negatively curved graphitic carbon networks containing heptagonal defects nearly twenty years ago, and have been recently extended to toroidal carbon nanotubes containing both heptagons and pentagons.[13] To experimentally approach these interesting negatively curved carbon structures, heptagon-embedded PAHs can serve as segments, models and, in principle, synthetic precursors. However, saddle-shaped PAHs that are embedded with seven-membered rings are very rare. To the best of our knowledge, [7]circulene[14] (shown in Figure 1a) and [7.7]-circulene[15] are the only known examples of such negatively curved π-molecules. Here we report a new saddle-shaped π-molecule (**1** shown in Figure 1a), which has a heptagon embedded in HBC. Unlike [7]circulene and [7.7]circulene, **1** has an sp^3 carbon atom in its seven-membered ring. This is similar to the bowl-shaped sumanene, which has an sp^3 carbon atom in each of its three five-membered rings.[16]

Another type of curved π-molecules explored here are alkoxylated hexabenzoperylenes **2a**,**b** as shown in Figure 1a. Like **1**, **2a**,**b** has the same number of Clar's aromatic sextets as HBC. Similar to hexabenzotriphenylene,[17] hexabenzoperylene

Received: June 5, 2012
Published: July 25, 2012

dx.doi.org/10.1021/ja3054354 | J. Am. Chem. Soc. 2012, 134, 13796−13803

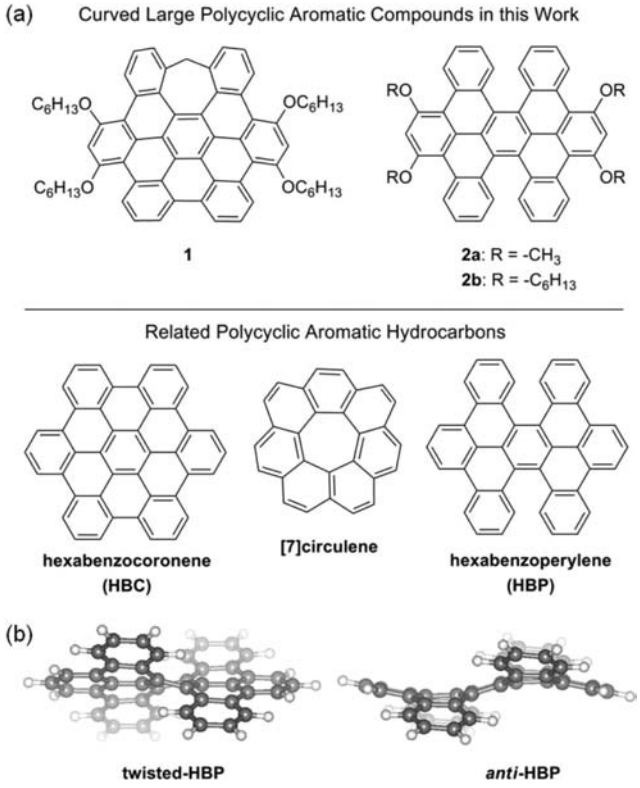

Figure 1. (a) Structures of curved large polycyclic aromatic compounds and related PAHs; (b) molecular models of twisted-HBP and *anti*-HBP as optimized at the B3LYP level of DFT with the 6-31G(d,p) basis set.

can be formally regarded as a partially hydrogenated HBC with opened bonds, and its curvature arises from overcrowding at its two fjord regions. They are even more curved than the earlier reported contorted hexabenzocoronene[18] because of the severer steric strains at the fjord regions. Unsubstituted hexabenzoperylene (HBP) was first synthesized by Clar et al. four decades ago[19] and reinvestigated by Ohshima et al. in 2004.[20] The recent computational study by Agranat et al.[21] indicates that HBP has two energy-minimum conformations, the chiral twisted conformation (twisted-HBP) at the global minimum and the *anti*-folded conformation (*anti*-HBP) at the local minimum as shown in Figure 1b. The D_2 symmetric twisted-HBP is calculated as more stable than the C_{2h} symmetric *anti*-HBP by 20.5 kJ/mol. Because the conversion between the two conformers is through a twisted-folded transition state, which is calculated higher than *anti*-HBP in energy by 114.7 kJ/mol, *anti*-HBP can in principle exist at room temperature. However, the kinetic stability of *anti*-HBP was not recognized in the previous studies,[20,21] and it was concluded that "only the twisted conformation of HBP exists a room temperature in solution".[21] The convenient synthesis of **2a**,**b** has led us to a comprehensive investigation on the twisted and *anti*-folded conformations of **2a**,**b** and their thermal isomerization as detailed below. Moreover, with suitable energy level of highest occupied molecular orbital (HOMO) and $\pi-\pi$ stacking, **2b** is found to function as a p-type semiconductor in organic thin film transistors (OTFTs).

RESULTS AND DISCUSSION

Synthesis. Shown in Scheme 1 is the synthesis of **1** starting from commercially available 3,5-dimethoxyphenylacetic acid.[22]

Scheme 1. Synthesis of Heptagon-Embedded HBC 1[a]

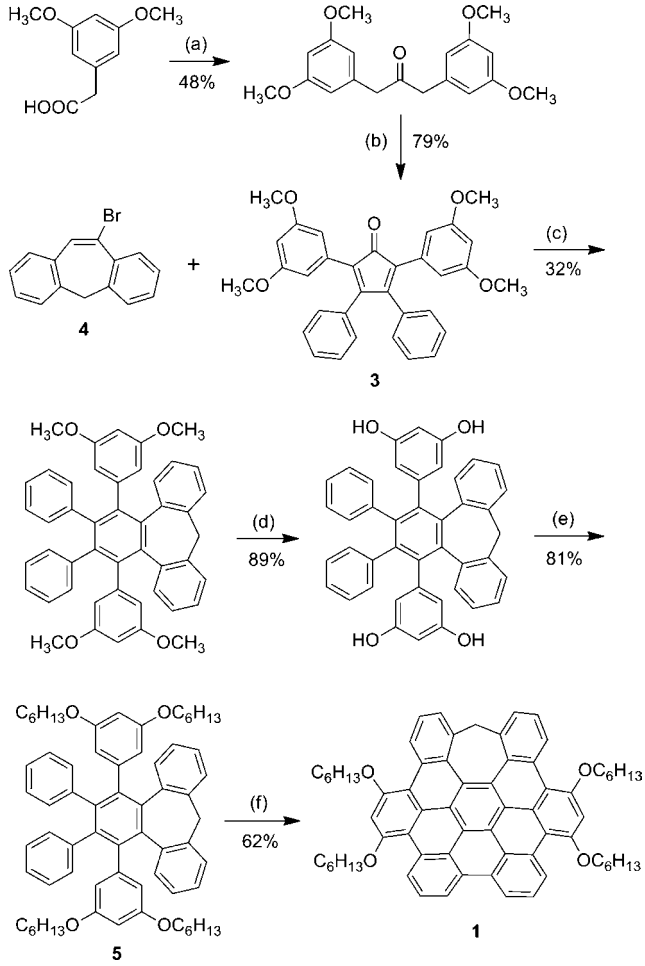

[a]Reagents and conditions: (a) DCC, DMAP, CH_2Cl_2; (b) 1,2-diphenylethane-1,2-dione, KOH, C_2H_5OH, reflux; (c) $(CH_3)_3COK$, ether; (d) BBr_3, CH_2Cl_2; (e) $C_6H_{13}Br$, K_2CO_3; (f) $FeCl_3$, CH_3NO_2, CH_2Cl_2, 3 h.

This synthesis was adapted from the well-known Müllen's synthesis of substituted HBCs[3] including Diels–Alder cycloaddition and Scholl-type oxidative cyclodehydrogenation as the key steps. The seven-membered ring was introduced from 10-bromo-5H-dibenzo[a,d]cycloheptene (**4**),[23] which generated a strained alkyne in situ as the dienophile in the Diels–Alder cycloaddition with cyclopentadienone **3**. After changing the methyl groups to hexyl groups to increase solubility of the final product, the resulting heptagon-containing hexaphenylbenzene **5** was then subjected to oxidative cyclodehydrogenation with $FeCl_3$ as both Lewis acid and oxidant. In this reaction, both the position of alkoxyl groups and the reaction time were found playing important roles. It was necessary to equip the heptagon-containing hexaphenylbenzene with alkoxyl groups *ortho* or *para* to the reaction sites since the Scholl reaction was reported to preferably form C–C bonds *ortho* or *para* to activating substituents.[24] Unlike **5**, the analogous precursors with alkoxyl groups *meta* to the reaction sites, **6** and **7** (shown in Chart 1), at the same condition yielded complex mixtures, from which the corresponding heptagon-embedded HBCs could not be isolated. It was found that the products of oxidative cyclodehydrogenation were highly dependent on the reaction time. When the reaction time was less than 2.5 h, an

dx.doi.org/10.1021/ja3054354 | J. Am. Chem. Soc. 2012, 134, 13796–13803

Chart 1. Precursors That Failed to Yield Heptagon-Embedded HBCs

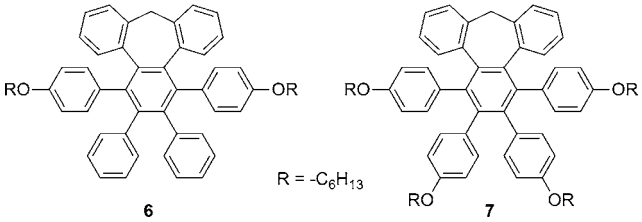

incompletely cyclized product **8** (shown in Chart 2) was found in the crude product and was difficultly removed from **1** by

Chart 2. Byproducts from Oxidative Cyclodehydrogenation of 5 with $FeCl_3$

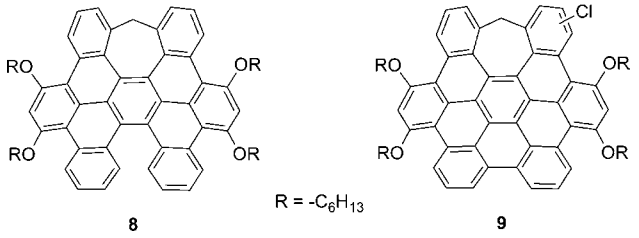

column chromatography or recrystallization. When the reaction time was prolonged to 3 h, the reaction yielded **1** (62%) along with a monochlorinated product **9** (37%) as shown in Chart 2. The exact position of chlorine in **9** was not determined based on its complicated ^{1}H NMR spectrum. Further prolongation of reaction time led to unknown products with lower yield of **1**. Moreover, the recently developed DDQ/CH_3SO_3H[25] was also tested in the oxidative cyclodehydrogenation, but only yielded the incompletely cyclized product **8** (67%).

Shown in Scheme 2 is the synthesis of **2a**,**b** starting from cyclopentadienone **3** following Müllen's strategy for synthesizing substituted HBCs. [3] Interestingly, the Scholl-type oxidative cyclodehydrogenation of tetraalkoxy-hexabenzobenzenes **10a** and **10b** with the recently developed DDQ/CH_3SO_3H[25] did not yield the corresponding HBCs but **2a** and **2b** as red solids, respectively. The possible reason for this incomplete cyclodehydrogenation is that the Scholl reaction is directed by the activating alkoxyl groups to form C−C bonds *ortho* or *para* to the activating substituents[24] first leading to the hexabenzoperylene backbone, which is too crowded at the fjord regions to allow two benzene rings getting close enough to form a C−C bond. In agreement with this hypothesis, **2a** and **2b** appeared inert toward oxidation by DDQ/CH_3SO_3H or $FeCl_3$. Due to its lower solubility, **2a** was more difficultly purified by column chromatography on silica gel leading to the lower isolated yield.

Structures and Properties of Heptagon-Embedded HBC 1. Heptagon-embedded HBC **1** is soluble in common organic solvents resulting in a yellow solution with green fluorescence when irradiated with UV light. Shown in Figure 2 (top) are the absorption and fluorescence spectra of **1** in CH_2Cl_2. In comparison to HBC and alkylated HBCs,[26] although **1** exhibits absorptions at very similar wavelengths, its absorption in the visible light region is much more intensive. The molar extinction coefficient of **1** at the longest-wavelength absorption (λ_{max} at 472 nm) is higher than that of HBC (λ_{max} at 463 nm) by 2 orders of magnitude.[27] Such enhanced absorption can be attributed to the lower symmetry of **1**

Scheme 2. Synthesis of Hexbenzoperylene 2a,b[a]

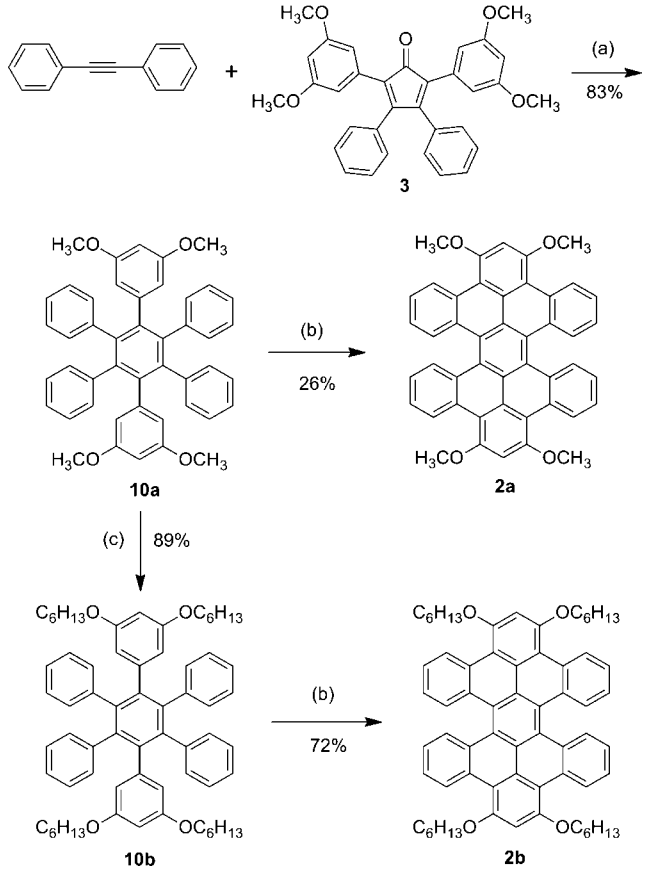

[a]Reagents and conditions: (a) diphenyl ether, reflux; (b) DDQ, CH_3SO_3H, CH_2Cl_2; (c) i. BBr_3, CH_2Cl_2; ii. K_2CO_3, $C_6H_{13}Br$, DMF.

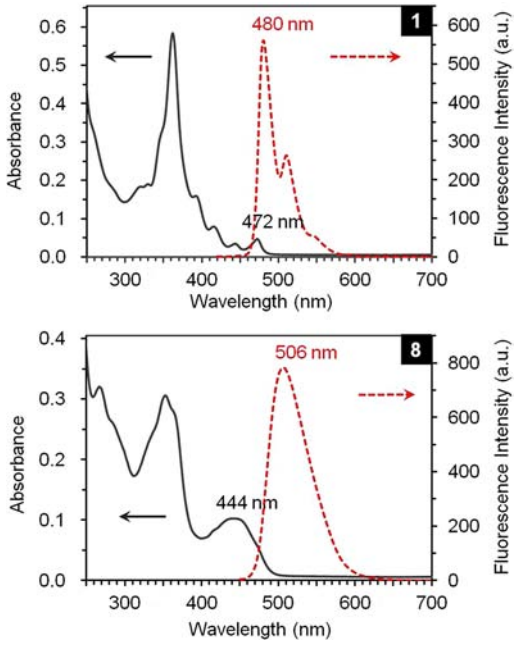

Figure 2. Absorption and fluorescence (excited at 410 and 440 nm, respectively) spectra of **1** (top) and **8** (bottom) in CH_2Cl_2 (5×10^{-6} mol/L).

since the very weak longest-wavelength absorption of HBC is known due to the strictly forbidden 0−0 transition in D_{6h}

dx.doi.org/10.1021/ja3054354 | J. Am. Chem. Soc. 2012, 134, 13796−13803

symmetry.[26,28] Unlike the substituted HBCs of lower symmetry, which have less than six alkyl or alkoxyl chains attached to the D_{6h} symmetric chromophore,[26,28] **1** has a curved π-backbone of C_s symmetry, leading to the stronger longest-wavelength absorption. The fluorescence spectra of **1** exhibits a small Stokes shift from 472 to 480 nm. Unlike **1**, the incompletely cyclized molecule **8** exhibits broad absorption bands without fine structures (vibrational details) and a much larger Stokes shift from 444 to 506 nm as shown in Figure 2 (bottom), both suggesting that **8** is more flexible than **1**.[29] This is in accordance with the fact that the incompletely cyclized structure of **8** can allow greater movement. The cyclic voltammogram of **1** in CH_2Cl_2 exhibits two reversible oxidation waves with half-wave oxidation potentials of 0.41 and 0.64 V vs ferrocenium/ferrocene. It does not exhibit any reduction waves in the testing window. From the first half-wave oxidation potential, the HOMO energy level of **1** is estimated as −5.21 eV.[30]

Single crystals of **1** were grown by slowly evaporating solvents from solutions in $CHCl_3$. Shown in Figure 3 is the crystal structure of **1**, which reveals that the π-backbone of **1** adopts a saddle shape of negative curvature. To quantify the curvature of the π-face of **1**, its Gauss curvature was calculated using the method detailed in the Supporting Information from the space coordinates of carbon atoms in the crystal structure.[31] Particularly, the benzylic sp^3 carbon in the seven-membered ring was excluded for the purpose of calculating curvature of the π-face of **1** as it is not a part of the sp^2 network. The total Gauss curvature for the π-face of **1** is calculated as −0.6483 sr, which is more negative than that of [7]circulene (−0.4857 sr).[32] The average Gauss curvature for the π-face of **1** is calculated as −0.01477 sr·Å^{-2}, which is slightly less negative than that of [7]circulene (−0.01736 sr·Å^{-2}) because **1** has a larger π-face. As highlighted in Figure 3b, the C−C bonds shown in blue have bond lengths close to those of the C−C single bonds shown in green. This can be attributed to the localization of π-bonds in the seven-membered ring. Moreover, the bonds shown in magenta are longer than the corresponding bonds in HBC by 0.013 to 0.022 Å. Such lengthened bonds may be related to distortion arising from the embedment of a heptagon in an originally flat π-molecule. Shown in Figure 3c is the molecular packing of **1**, which interestingly does not exhibit $\pi-\pi$ interactions between the two neighboring curved π-faces. The distance between the two curved π-faces is 8.72 Å as measured from the distance between the two least-squares planes of central benzene rings. The space between the two curved π-faces is occupied by alkyl side chains. The absence of π-interactions between molecules of **1** in principle prevents its application as an organic semiconductor in the solid state.

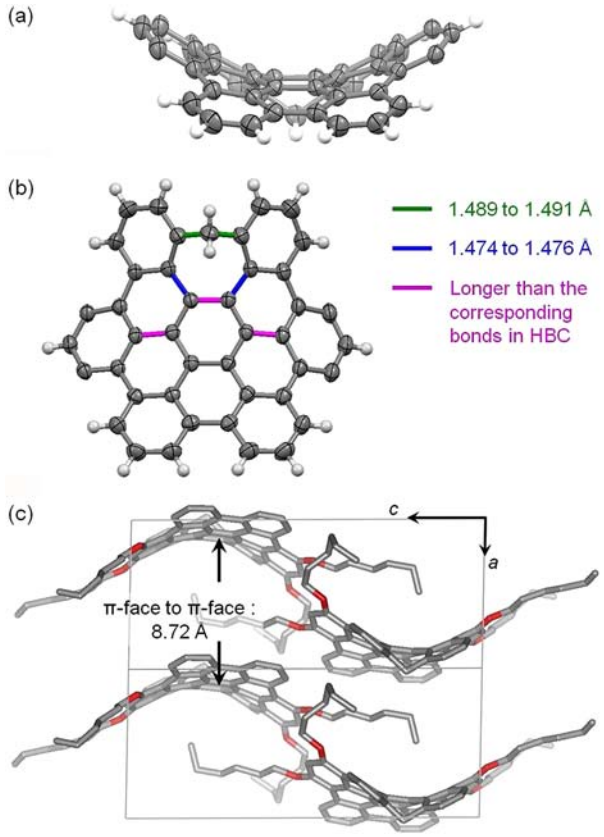

Figure 3. Crystal structure of **1**. (a) Side view and (b) top view of the π-backbone of **1** with the hexyloxyl groups removed and carbon atom positions shown as 50% probability ellipsoids; (c) molecular packing of **1** as viewed along the *b* axis of the unit cell with hydrogen atoms removed for clarity. (Carbon, oxygen, and hydrogen atoms are shown in gray, red, and white, respectively.).

The π-backbone of **1** is in principle able to invert itself in a way similar to the saddle-to-saddle inversion of [7]circulene, which is through a planar transition state with a small activation energy of about 36 kJ/mol as indicated by an early computational study.[33] As **1** has two chemically different protons in its seven-membered ring and the two protons interconvert during the inversion process, variable temperature ^{1}H NMR spectroscopy can be conveniently used to monitor the saddle-to-saddle inversion of **1** in solution. In this study, the ^{1}H NMR spectra of **1** in $CDCl_3$ from 25 to 55 °C and in DMSO-d_6 from 90 to 150 °C were recorded due to the low solubility of **1** in DMSO-d_6 at lower temperature. In the two temperature ranges, the benzylic protons in the seven-membered ring of **1** exhibited a pair of well-resolved doublet signals (at 3.72 and 4.09 ppm in $CDCl_3$, and at 3.58 and 4.22 ppm in DMSO-d_6) without movement and broadening of signals as shown in the Supporting Information. This indicates that the saddle-to-saddle inversion of **1** is a slow process compared to the NMR time scale or does not occur in the temperature range tested here. Taking an assumption that the two signals reached coalescence at 150 °C, an exchange rate could be estimated as 329 S^{-1} using $k = \pi\Delta\nu/\sqrt{2}$, where $\Delta\nu$ =148 Hz is the frequency separation of the two signals under the condition of slow exchange as measured in $CDCl_3$. This exchange rate would lead to an activation free energy of 84 kJ/mol at 150 °C.[34] Therefore the activation free energy for the saddle-to-saddle inversion of **1** must be higher than 84 kJ/mol, indicating that **1** has a rigid π-backbone, which inverts itself much more difficultly than [7]circulene does. This conclusion is also in agreement with the finding that **1** shows fine structures in the UV−vis absorption spectrum with a small Stokes shift. In contrast, the benzylic protons in the seven-membered ring of **8** exhibited a pair of well-resolved doublet signals at −20 °C but two broad peaks at room temperature. This is in agreement with the finding that the incompletely cyclized structure of **8** is more flexible.

Conformation and Isomerization of Hexabenzoperylenes 2a and 2b. Although *anti*-HBP is less stable than twisted-HBP by 20.5 kJ/mol as calculated by Agranat et al.,[21] it can be kinetically stable because the conversion between the

dx.doi.org/10.1021/ja3054354 | J. Am. Chem. Soc. 2012, 134, 13796−13803

two conformers is through a twisted-folded transition state, which is higher than *anti*-HBP in energy by 114.7 kJ/mol as calculated. The early synthesized HBP was reported as twisted-HBP,[20] while *anti*-HBP was not experimentally achieved. With the red crystals of hexbenzoperylenes **2a**,**b** in hand, we became interested in the following two questions: Do **2a**,**b** exist as the twisted or the *anti*-folded conformation? Can **2a**,**b** convert to their isomers by changing the conformation of their π-backbone at elevated temperature?

To answer the first question, crystals of **2a**,**b** were grown from solutions by slow evaporation of solvents, but only the red crystals of **2a** grown from CH_2Cl_2 were qualified for single-crystal X-ray crystallography, which revealed the chiral twisted conformation of **2a**. The unit cell of this crystal contains two pairs of enantiomers of twisted-**2a** together with crystallized solvent molecules as shown in Figure 4a. In the crystal of twisted-**2a**•CH_2Cl_2, the geometry of twisted-**2a** is essentially the same as the DFT energy-minimized model except that it slightly deviates from the D_2 symmetry by having unequal torsion angles in the two fjord regions possibly due to the experimental errors. As shown in Figure 4b, the torsion angles as defined by the three magenta bonds in the fjord regions are 42.1° and 39.2°, which are in good agreement with the torsion angle of 40.9° as found in the DFT energy minimized model. As indicated by the red and blue arrows in Figure 4c, neighboring molecules of twisted-**2a** interact with each other in both face-to-face and edge-to-face modes.[35] A neighboring pair of enantiomers of twisted-**2a** stack in a face-to-face arrangement with the two curved π-faces separated by about 3.6 Å as measured from two parallel least-squares planes of benzene rings. Two neighboring twisted-**2a** molecules of the same handedness interact with each other in an edge-to-face arrangement with three intermolecular carbon−carbon contacts within the range of 3.61 to 3.85 Å.[36] Because the red compounds **2a** and **2b** exhibit almost identical UV−vis absorption spectra and ^{1}H NMR spectra in the aromatic range, it is concluded that the as-synthesized **2b** is also the twisted conformer (twisted-**2b**).

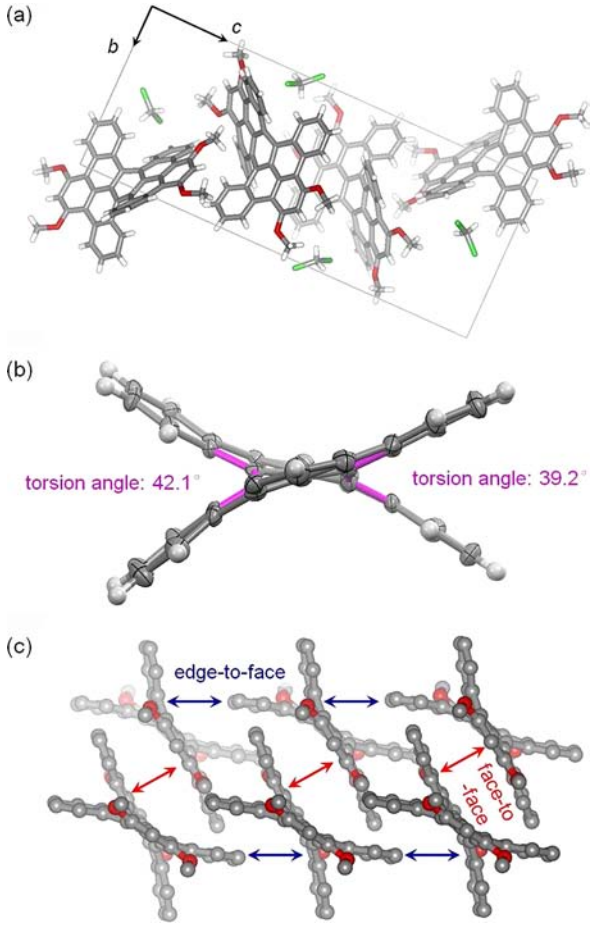

Figure 4. Crystal structure of twisted-**2a**•CH_2Cl_2: (a) a unit cell of twisted-**2a** viewed along the *a* axis showing the crystallized CH_2Cl_2 molecules; (b) π-backbone of twisted-**2b** with the methoxyl groups removed and carbon atom positions shown as 50% probability ellipsoids; (c) $\pi-\pi$ interactions between neighboring molecules of twisted-**2a** with hydrogen atoms removed for clarity. (Carbon, oxygen, hydrogen, and chloroine atoms are shown in gray, red, white, and green, respectively.).

To test whether twisted-**2a** and twisted-**2b** can isomerize to their *anti*-folded conformers, we then optimized the twisted and *anti*-folded conformers of **2a** and HBP at the B3LYP level of DFT with the 6-31G(d,p) basis set and calculated their highest occupied molecular orbitals (HOMOs) and lowest unoccupied molecular orbitals (LUMOs) with the 6-311++G(d,p) basis set. As summarized in Table 1, the calculated energy for the twisted conformer of **2a** (twisted-**2a**) is only slightly lower than that of *anti*-folded conformer (*anti*-**2a**) by 0.67 kJ/mol, while the calculated energy difference between twisted-HBP and *anti*-HBP is 19.32 kJ/mol, which is the same as that calculated by Agranat et al. when using the same basis set.[21] This large shift of relative stability of the twisted isomer upon going from unsubstituted HBP to **2a** is presumably related to a steric repulsion between the oxygen atom and the neighboring aromatic hydrogen atom as shown in the Supporting Information. As measured from energy-minimized models, such steric repulsion involves an H-to-O distance of 2.07 Å in twisted-**2a** and 2.16 Å in *anti*-**2a**. These distances are shorter than the sum of van der Waals radii by about 0.5 Å and suggest that twisted-**2a** is destabilized by the steric repulsion in a larger degree. The most interesting finding from Table 1 is that the twisted conformers have a smaller HOMO−LUMO gap than the corresponding *anti*-folded conformers, predicting that *anti*-**2a** and *anti*-**2b** would have blue-shifted absorption in comparison with their twisted isomers. The different HOMO−LUMO gaps of twisted and *anti*-folded conformers may be related to the different distributions of electrons on the central benzene ring, which is more distorted in the twisted conformer.[21] A similar effect was observed earlier in some

Table 1. Relative Energy and Energy Levels of HOMO and LUMO for Twisted and *anti*-Folded Conformers of 2a and HBP as Calculated at the B3LYP Level of DFT[a]

	twisted-**2a**	*anti*-**2a**	twisted-HBP	*anti*-HBP
relative energy (kJ/mol)[b]	0	0.67	0	19.32
HOMO (eV)	−4.78	−4.92	−5.34	−5.46
LUMO (eV)	−2.05	−1.76	−2.41	−2.16
HOMO−LUMO gap (eV)	2.73	3.16	2.93	3.30

[a]The relative energy was optimized with the 6-31G(d,p) basis set, and the energy levels of HOMO and LUMO were calculated with the 6-311++G(d,p) basis set. [b]The energy of twisted-**2a** and twisted-HBP is set as 0.

dx.doi.org/10.1021/ja3054354 | J. Am. Chem. Soc. 2012, 134, 13796−13803

overcrowded bistricyclic aromatic enes, which exist as a colorless or yellow *anti*-folded conformer at room temperature and convert to a deep-blue or deep-green twisted conformer at higher temperature.[37] Another finding from Table 1 is that substitution with alkoxyl groups reduces the HOMO−LUMO gap of hexbenzoperylene as the electron-donating substituents raise HOMO by a larger degree than raising LUMO.

As suggested by the transition state connecting twisted-HBP and *anti*-HBP calculated by Agranat et al.,[21] and the small energy difference between twisted-**2a** and *anti*-**2a** calculated above, heating the twisted isomer of **2a**,**b** would result in a mixture of the twisted isomer and the *anti*-folded isomer. Following this prediction, we heated twisted-**2a** and twisted-**2b** in toluene. Heating twisted-**2a** led to a new compound together with twisted-**2a** as found from the thin layer chromatography. The ^{1}H NMR spectrum of the crude product suggested that this new compound might be an isomer of twisted-**2a**, which unfortunately could not be isolated from the crude product by column chromatography or recrystallization for full characterization. In contrast, refluxing a solution of twisted-**2b** in toluene under an atmosphere of nitrogen for 1 h led to a new yellow compound together with twisted-**2b**. This yellow compound was conveniently isolated from the mixture by chromatography on silica gel and was determined as an isomer of twisted-**2b** based on the ^{1}H NMR and mass spectra.[38] Shown in Figure 5

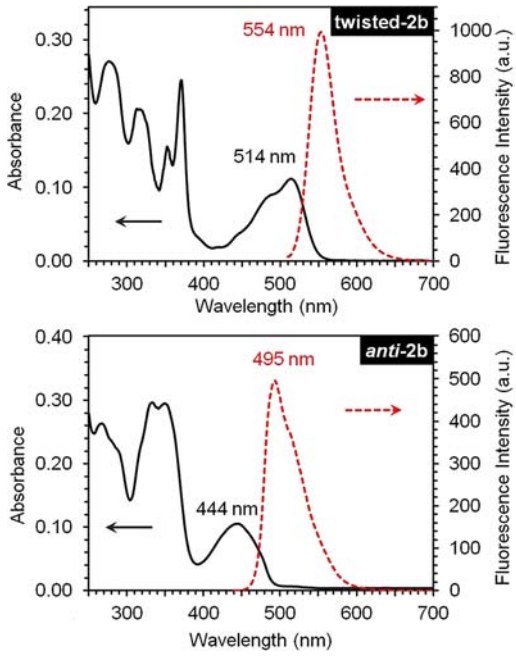

Figure 5. Absorption and fluorescence (excited at 500 and 430 nm, respectively) spectra of twisted-**2b** (top) and *anti*-**2b** (bottom) in CH_2Cl_2 (5×10^{-6} mol/L).

are the absorption and fluorescence spectra of twisted-**2b** and its yellow isomer in CH_2Cl_2. Compared with the reported spectrum of twisted-HBP, the absorption of twisted-**2b** has almost the same shape but shifts to red by about 50 nm.[39] Such red shift is in agreement with DFT calculation that the electron-donating alkoxyl substituents reduce the HOMO−LUMO gap. On the other hand, the yellow isomer of twisted-**2b** exhibits absorption bands of different shape. The longest-wavelength absorption of this yellow isomer shifts to blue by about 70 nm relative to that of twisted-**2b**. Because the DFT calculation indicates that *anti*-**2b** would have blue-shifted absorption in comparison with twisted-**2b**, we assign the *anti*-folded conformation to the yellow isomer of twisted-**2b**. From the longest-wavelength absorption, the optical gap of *anti*-**2b** is determined as 2.80 eV, which is 0.39 eV greater than that of twisted-**2b**. Such difference agrees quantitatively with the DFT calculation that the HOMO−LUMO gaps of *anti*-**2a** and *anti*-HBP are greater than those of their twisted isomers by about 0.4 eV.

Not only the UV−vis absorption but also the electrochemistry of the twisted and *anti*-folded isomers of **2b** exhibit apparent difference. The cyclic voltammogram of twisted-**2b** in CH_2Cl_2 (shown in the Supporting Information) exhibits one reversible reduction wave, which has the half-wave potential at −2.04 V vs ferrocenium/ferrocene, and two reversible oxidation waves, which have the half-wave potential at 0.22 and 0.50 V vs ferrocenium/ferrocene. From the first oxidation potential and reduction potential, the HOMO and LUMO energy levels of twisted-**2b** are estimated as −5.02 and −2.76 eV, respectively.[30] In contrast, the cyclic voltammogram of *anti*-**2b** exhibits no reduction waves in the testing window but only two reversible oxidation waves, which have the half-wave potential at 0.34 and 0.57 V vs ferrocenium/ferrocene. From the first oxidation potential, the HOMO energy level of *anti*-**2b** is estimated as −5.14 eV.[30] The higher oxidation potentials and absence of reduction wave in the cyclic voltammogram of *anti*-**2b** are in agreement with the DFT calculation that the *anti*-folded isomer has higher HOMO and LUMO energy levels than the twisted isomer as shown in Table 1.

To better understand the stability of the two isomers of **2b**, we studied the thermodynamics and kinetics of the thermal isomerization using ^{1}H NMR spectroscopy. Heating a solution of either pure twisted-**2b** or pure *anti*-**2b** in toluene at 110 °C for 1 h led to the same equilibrium mixture of twisted-**2b** and *anti*-**2b** in a ratio of 1: 0.35, which was easily determined from the integrations in the ^{1}H NMR spectra of the mixture as shown in Figure 6a. From this ratio, the free energy change ΔG for the twisted-to-*anti* isomerization is calculated as 3.3 kJ/mol, which is qualitatively in agreement with the calculated results that the *anti*-folded isomer is less stable. Because *anti*-**2b** is less soluble than twisted-**2b**, the most effective way to prepare *anti*-**2b** is to boil a solution of twisted-**2b** in toluene without a condenser allowing part of the solvent to evaporate. In this way, precipitation of *anti*-**2b** as yellow powders shifts the equilibrium leading to a higher yield of *anti*-**2b**. The thermal isomerization of twisted-**2b** is a reversible unimolecular reaction, and its rate constants can be estimated by using the equation $\ln([x]_e/([x]_e - [x])) = (k_f + k_r)t$ or its equivalent form, $-\ln(1 - [x]/[x]_e) = (k_f + k_r)t$, where $[x]$ is the concentration of twisted-**2b** that has been depleted at a certain time t representing the extent of reaction, $[x]_e$ is defined as $[x]$ at equilibrium, k_f and k_r are the rate constants for the forward and reverse reactions, respectively.[40] In the kinetic experiment, a solution of twisted-**2b** in toluene-d_8 was heated at 110 °C in a sealed NMR tube, and the progress of twisted-to-*anti* isomerization was monitored with ^{1}H NMR spectroscopy. The integrations of the two sets of peaks were used to calculate the ratio of $[x]_e/[x]$. Ploting $-\ln(1 - [x]/[x]_e)$ versus time leads to a slope of 1.48×10^{-3} s^{-1} as shown in Figure 6b. From this slope and the reaction equilibrium constant $K = k_f/k_r = 0.35$, the rate constants k_f and k_r at 110 °C are determined as 3.8×10^{-4} s^{-1} and 1.1×10^{-3} s^{-1}, respectively. Using the Eyring equation $k = \kappa(k_B T/h)\exp(-\Delta G^{\ddagger}/RT)$ and assuming a value of unity for the

dx.doi.org/10.1021/ja3054354 | J. Am. Chem. Soc. 2012, 134, 13796−13803

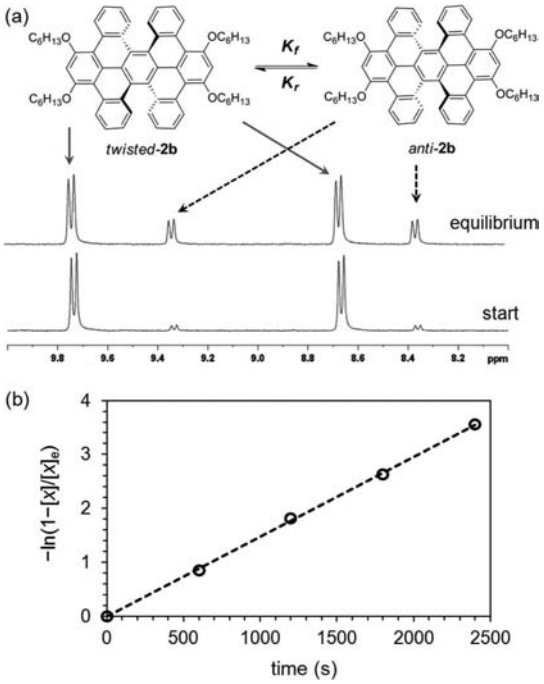

Figure 6. Isomerization of **2b** as monitored by ^{1}H NMR (400 MHz) spectroscopy: (a) selected ^{1}H NMR spectra of twisted-**2b** and *anti*-**2b** during the progress of twisted-to-*anti* isomerization in toluene-d_8 at 110 °C; (b) a plot of $-\ln(1 - [x]_e/[x])$ for twisted-**2b** versus time.

transmission coefficient (κ),[40] the activation free energy $\Delta G^{\ddagger}$ is calculated as 120 kJ/mol for the twisted-to-*anti* isomerization and 116 kJ/mol for the *anti*-to-twisted isomerization, which is in agreement with the calculated energy barrier for *anti*-HBP (114.7 kJ/mol).[21]

Semiconductor Properties. To explore the potential of the curved π-molecules as semiconductors, we tested **1**, twisted-**2b**, and *anti*-**2b** in thin film transistors. Because of the thermal isomerization of twisted-**2b** and *anti*-**2b**, thin films of these compounds were fabricated not by thermal evaporation, which requires high temperature, but by solution process at much lower temperature. To fabricate thin film transistors, a solution of **1**, twisted-**2b**, or *anti*-**2b** in chlorobenzene was drop-cast onto a silicon wafer, which had its SiO_2 surface pretreated with a self-assembled monolayer of hexamethyldisilazane (HMDS) and had its predeposited bottom-contact gold source and drain electrodes modified with a self-assembled monolayer of pentafluorobenzenethiol (PFBT).[41] Under the drop-casting condition, the isomerization of twisted-**2b** or *anti*-**2b** was negligible because the solution was heated at 60 °C within only 30 s before the solvent evaporated completely. This was supported by the ^{1}H NMR spectra from the solutions of these films, from which the corresponding isomers were not observed. The drop-cast films of **1** and twisted-**2b** were composed of connected crystallites, while those of anti-**2b** only contained isolated crystallites of larger size. Because the isolated crystallites of anti-**2b** were not able to form continuous pathway for charge transport, the films of anti-**2b** appeared insulating. Unlike its *anti*-folded isomer, twisted-**2b** performed as a p-type semiconductor in the thin films with a field effect mobility of 5×10^{-5} to 2×10^{-4} cm^2 V^{-1} s^{-1}. This semiconductor property is in agreement with the suitable HOMO energy level of twisted-**2b** and a sufficient $\pi-\pi$ stacking as suggested by the crystal structure of twisted-**2a**. The low mobility of twisted-**2b** very possibly arises from the large number of grain boundaries between small crystallites. On the other hand, the films of **1** behaved as an insulator, which can be attributed to the absence of $\pi-\pi$ interactions in its solid state.

CONCLUSION

In summary, this study has explored how the properties of curved π-molecules depend on their curvature by synthesizing and characterizing two types of curved π-molecules that are π-isoelectronic to the planar HBC. They are forced out of planarity either by an embedded seven-membered ring or by atom crowding at the fjord region. The successful synthesis of these compounds is related to introducing alkoxyl groups to unprecedented positions of hexaphenylbenzenes. Embedding a heptagon in HBC leads to a novel saddle-shaped molecule **1**, whose π-backbone is slightly less curved than the previously reported [7]circulene in terms of the average Gauss curvature, but surprisingly much more rigid than [7]circulene. Overcrowded fjord regions in novel derivatives of hexabenzoperylene (HBP) **2a**,**b** lead to chiral twisted and *anti*-folded conformers, which exhibit different photophysical and electrochemical properties. Red twisted-**2b** converts at elevated temperature to its yellow isomer, *anti*-**2b**, with an activation free energy of 120 kJ/mol. The red-shifted absorption of twisted conformer may be attributed to the severer distortion of its central benzene ring, which leads to redistribution of electrons in HOMO and LUMO. These findings have improved the early understandings on the conformation of HBP. Unlike **1**, which lacks $\pi-\pi$ interactions in the solid state, **2a** exhibits both face-to-face and edge-to-face $\pi-\pi$ interactions. It is found that twisted-**2b** functions as a p-type semiconductor in thin film transistors, while the thin films of **1** appear insulating presumably due to lacking $\pi-\pi$ interactions. In view of the three different types of curvatures in **1** and the two isomers of **2b**, we come to the conclusion that the curvature of π-face plays a role in determining the frontier molecular orbital energy levels and $\pi-\pi$ interactions and thus needs to be considered when one designs new organic semiconductors.

ASSOCIATED CONTENT

Supporting Information

Details of synthesis and characterization, the crystallographic information files (CIF) for **1** and twisted-**2a**, fabrication and characterization of organic thin film transistors, NMR spectra, and calculation of the Gauss curvature. This material is available free of charge via the Internet at http://pubs.acs.org.

AUTHOR INFORMATION

Corresponding Author

miaoqian@cuhk.edu.hk

Notes

The authors declare no competing financial interest.

ACKNOWLEDGMENTS

We sincerely thank Dr. Yi Liu (Department of Mathematics, University of California, Berkeley) for the calculation on Gauss curvature and Ms. Hoi Shan Chan (Department of Chemistry, the Chinese University of Hong Kong) for the single crystal crystallography. This work was supported by the University Grants Committee of Hong Kong (project number AoE/P-03/08) and the Research Grants Council of Hong Kong (project number GRF402412).

REFERENCES

(1) Bharat; Bhola, R.; Bally, T.; Valente, A.; Cyrański, M. K.; Dobrzycki, Ł.; Spain, S. M.; Rempała, P.; Chin, M. R.; King, B. T. *Angew. Chem., Int. Ed.* **2010**, *49*, 399.

(2) Rieger, R.; Müllen, K. *J. Phys. Org. Chem.* **2010**, *23*, 315.

(3) (a) Wu, J.; Pisula, W.; Müllen, K. *Chem. Rev.* **2007**, *107*, 718. (b) Zhi, L.; Müllen, K. *J. Mater. Chem.* **2008**, *18*, 1472.

(4) Wu, Y. T.; Siegel, J. S. *Chem. Rev.* **2006**, *106*, 4843.

(5) For recent examples, see: (a) Steinberg, B. D.; Jackson, E. A.; Filatov, A. S.; Wakamiya, A.; Petrukhina, M. A.; Scott, L. T. *J. Am. Chem. Soc.* **2009**, *131*, 10537. (b) Amaya, T.; Nakata, T.; Hirao, T. *J. Am. Chem. Soc.* **2009**, *131*, 10810. (c) Whalley, A. C.; Plunkett, K. N.; Gorodetsky, A. A.; Schenck, C. L.; Chiu, C.-Y.; Steigerwald, M. L.; Nuckolls, C. *Chem. Sci* **2011**, *2*, 132. (d) Wu, T. C.; Hsin, H. J.; Kuo, M. Y.; Li, C. H.; Wu, Y. T. *J. Am. Chem. Soc.* **2011**, *133*, 16319.

(6) Rabideau, P. W.; Sygula, A. *Acc. Chem. Res.* **1996**, *29*, 235.

(7) Scott, L. T. *Angew. Chem., Int. Ed.* **2004**, *43*, 4994.

(8) (a) Fort, E. H.; Donovan, P. M.; Scott, L. T. *J. Am. Chem. Soc.* **2009**, *131*, 16006. (b) Scott, L. T.; Jackson, E. A.; Zhang, Q.; Steinberg, B. D.; Bancu, M.; Li, B. *J. Am. Chem. Soc.* **2011**, *134*, 107. (c) Fort, E. H.; Scott, L. T. *J. Mater. Chem.* **2011**, *21*, 1373.

(9) For a layman's explanation of positive and negative curvature, see: Gamow, G. *One, Two, Three—Infinity*; Viking Press: New York, 1961; Chapter V.

(10) Kerner, R. In *Topology in Condensed Matter*; Monastyrsky, M. I., Ed.; Spinger, 2006; Chapter 3.2.

(11) Lenosky, T.; Gonze, X.; Teter, M.; Elser, V. *Nature* **1992**, *355*, 333.

(12) Iijima, S.; Ichihashi, T.; Ando, Y. *Nature* **1992**, *356*, 776.

(13) Beuerle, F.; Herrmann, C.; Whalley, A. C.; Valente, C.; Gamburd, A.; Ratner, M. A.; Stoddart, J. F. *Chem.—Eur. J.* **2011**, *17*, 3868.

(14) (a) Yamamoto, K.; Harada, T.; Nakazaki, M. *J. Am. Chem. Soc.* **1983**, *105*, 7171. (b) Yamamoto, K.; Harada, T.; Okamoto, Y.; Chikamatsu, H.; Nakazaki, M.; Kai, Y.; Nakao, T.; Tanaka, M.; Harada, S.; Kasai, N. *J. Am. Chem. Soc.* **1988**, *110*, 3578.

(15) (a) Yamamoto, K.; Saitho, Y.; Iwaki, D.; Ooka, T. *Angew. Chem., Int. Ed.* **1991**, *30*, 1173. (b) Yamamoto, K. *Pure Appl. Chem.* **1993**, *65*, 157.

(16) (a) Sakurai, H.; Daiko, T.; Hirao, T. *Science* **2003**, *301*, 1878. (b) Amaya, T.; Hirao, T. *Chem. Commun.* **2011**, *47*, 10524. (c) Higashibayashi, S.; Sakurai, H. *J. Am. Chem. Soc.* **2008**, *130*, 8592.

(17) (a) Barnett, L.; Ho, D. M.; Baldridge, K. K.; Pascal, R. A., Jr. *J. Am. Chem. Soc.* **1999**, *121*, 727. (b) Peña, D.; Pérez, D.; Guitián, E.; Castedo, L. *Org. Lett.* **1999**, *1*, 1555.

(18) Xiao, S.; Myers, M.; Miao, Q.; Sanaur, S.; Pang, K.; Steigerwald, M.; Nuckolls, C. *Angew. Chem., Int. Ed.* **2005**, *44*, 7390.

(19) (a) Clar, E.; Ironside, C. T.; Zander, M. *J. Chem. Soc.* **1959**, 142. (b) Clar, E. *The Aromatic Sextet*; Wiley: New York, 1972.

(20) Fujimaki, Y.; Takekawa, M.; Fujisawa, S.; Ohshima, S.; Sakamoto, Y. *Polycyclic Aromat. Compd.* **2004**, *24*, 107.

(21) Marom, H.; Pogodin, S.; Agranat, I. *Polycyclic Aromat. Compd.* **2007**, *27*, 295.

(22) An alternative synthesis involving the same number of steps is to start with alkylation of methyl 3,5-dihydroxyphenylacetate with 1-bromohexane. The synthesis route shown in Scheme 1 was chosen so that varied alkyl groups could be attached to the π-backbone at the end of the synthesis without preparing varied starting materials for every target molecule.

(23) Phillips, S. T.; Depaulis, T.; Neergaard, J. R.; Baron, B. M.; Siegel, B. W.; Seeman, P.; Van Tol, H. H. M.; Guan, H. C.; Smith, H. E. *J. Med. Chem.* **1995**, *38*, 708.

(24) King, B. T.; Kroulik, J.; Robertson, C. R.; Rempala, P.; Hilton, C. L.; Korinek, J. D.; Gortari, L. M. *J. Org. Chem.* **2007**, *72*, 2279.

(25) Zhai, L. Y.; Shukla, R.; Rathore, R. *Org. Lett.* **2009**, *11*, 3474.

(26) Hendel, W.; Khan, Z. H.; Schmidt, W. *Tetrahedron* **1986**, *42*, 1127.

(27) The molar extinction coefficient of **1** at 472 nm is 4.22×10^4 L mol^{-1} cm^{-1}, while the molar extinction coefficient of **1** at 463 nm is 220 L mol^{-1} cm^{-1} as reported in ref 26.

(28) Wang, Z.; Waston, M. D.; Wu, J.; Müllen, K. *Chem. Commun.* **2004**, 336.

(29) Anslyn, E. V.; Dougherty, D. A.; *Modern Physical Organic Chemistry*; University Science Books: Sausalito, 2004; Chapter 16.

(30) The commonly used HOMO energy level of ferrocene is −4.80 eV. See: (a) Pommerehne, J.; Vestweber, H.; Guss, W.; Mahrt, R. F.; Bässler, H.; Porsch, M.; Daub, J. *Adv. Mater.* **1995**, *7*, 551. (b) D'Andrade, B. W.; Datta, S.; Forrest, S. R.; Djurovich, P.; Polikarpov, E.; Thompson, M. E. *Org. Electron.* **2005**, *6*, 11.

(31) This calculation was done by Dr. Yi Liu (Department of Mathematics, University of California, Berkeley).

(32) The Gauss curvature of [7]circulene was calculated using the same method from the space coordinates of carbon atoms in the crystal structure reported by Goddard, R.; Haenel, M. W.; Herndon, W. C.; Krüger, C.; Zander, M. *J. Am. Chem. Soc.* **1995**, *117*, 30.

(33) Shen, M.; Ignatyev, I. S.; Xie, Y.; Schaefer, H. F., III. *J. Phys. Chem.* **1993**, *97*, 3212.

(34) The activation free energy of 84 kJ/mol is calculated by using the Eyring equation $k = \kappa(k_B T/h)\exp(-\Delta G^{\ddagger}/RT)$ and assuming a value of unity for the transmission coefficient (κ).

(35) A combination of face-to-face and edge-to-face π-π interactions are also found in the crystals of other curved π-molecules. For example, see: Xia, H.; Liu, D.; Song, K.; Miao, Q. *Chem. Sci* **2011**, *2*, 2402.

(36) Intermolecular carbon-carbon contacts within in the range of 3.5 to 3.92 Å were considered as short contacts between neighboring pentacene molecules in crystals, see: Siegrist, T.; Kloc, C.; Schön, J. H.; Ballogg, B.; Haddon, R. C.; Berg, S.; Thomas, G. A. *Angew. Chem. Int. Ed.* **2001**, *40*, 1732.

(37) Biedermann, P. U.; Stezowski, J. J.; Agranat, I. *Chem.—Eur. J.* **2006**, *12*, 3345.

(38) This yellow isomer of twisted-**2b** exhibits a molecular ion peak of m/z = 926.5288, the same as that of twisted-**2b**, and five sets of signals in the aromatic range of ^{1}H NMR spectrum. These signals shift to the upfield and have the same patterns in comparison to those of twisted-**2b**.

(39) To avoid the influence of solvent, we also collected the absorption and fluorescence spectra of twisted-**2b** from solution in benzene, the same solvent used for the spectra of twisted-HBP as reported in ref 20. As shown in the Supporting Information, the spectra of **2b** in benzene are essentially identical to those in CH_2Cl_2 indicating that the red shift of **2b** is not dependent on the solvent. For comparison, the spectrum of HBP copied from ref 20 is also shown in the Supporting Information.

(40) Anslyn, E. V.; Dougherty, D. A. *Modern Physical Organic Chemistry*; University Science Books: Sausalito, 2004; Chapter 7.

(41) Park, S. K.; Jackson, T. N.; Anthony, J. E.; Mourey, D. A. *Appl. Phys. Lett.* **2007**, *91*, 063514.

NOTE ADDED AFTER ASAP PUBLICATION

This paper was published ASAP on August 8, 2012. Changes were made in the first full paragraph on the fourth page and in Reference 27. The revised version was posted on August 13, 2012.